Fuel 407 (2026) 137564

Contents lists available at ScienceDirect

Fuel

journal homepage: www.elsevier.com/locate/fuel

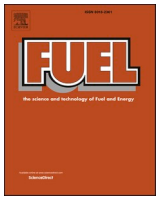

Full Length Article

Thermochemical valorisation of real post-consumer mixed textile waste

Surika van Wyk *, Carlos F. Mourao Vilela, Berend J. Vreugdenhil

Biobased and Circular Technology Group, Energy & Materials Transition Unit, The Netherlands Organization for Applied Scientific Research (TNO), Petten, the Netherlands

ARTICLE INFO

Keywords:
Textiles
Thermochemical recycling
Fluidized bed
Waste valorisation
Syngas
BTX

ABSTRACT

Thermochemical conversion for the valorisation of mixed post-consumer textile waste was experimentally investigated. Four model mixtures were investigated, mainly consisting of polyethylene terephthalate (PET) with the addition of nylon (polyamide (PA) 6) and elastane (polyurethane (PUR)), to represent the synthetic fraction of textiles, and one real post-consumer textile waste stream. Experiments were performed in a bubbling fluidized bed for different temperatures (700–850 °C) and steam-to-carbon ratios (0 & 1). Due to the thermal decomposition of PET, the main products were CO_2 (15 % carbon yield) and benzene (26 % carbon yield) for the model mixtures. With the addition of PA6 and PUR, the yields decreased in favour of higher hydrocarbon yields. For the real textile waste (>50 wt% cotton), the product distribution shifted towards higher product gas yields, with the gas mainly consisting of syngas (H_2 and CO). As the reaction temperature increased the benzene, toluene and light olefin yields for the real textile waste increased (up to 802 °C). At higher temperatures syngas became the predominant product, with H_2 yields increasing significantly. The effect of steam on the product distribution was less significant compared to the reaction temperatures, with steam leading to higher H_2 and CO_2 yields. The results demonstrated the feasibility of textile waste valorisation via thermochemical conversion to retrieve high-value chemicals (benzene and toluene) and syngas with varying compositions.

1. Introduction

Textile waste is the third largest contributor to global plastic waste, after the packaging and construction sector [1]. In 2017 the Global Fashion Agenda and the Boston Consulting Group reported that 92 million tons of textile waste was generated in 2015 and it was projected to increase to 148 million tons in 2030 (62 % increase) [2]. Only 1 % of textile waste is currently recycled to produce new clothing (closed-loop recycling), while 12 % is downcycled for lower value applications and 14 % is lost during production and collection. The remaining 73 % is either landfilled or incinerated, contributing to CO_2 emissions, soil pollution, ground water contamination and loss of valuable carbon [3,4]. The increasing global population and the rise of fast fashion, coupled with production of low-quality garments and their premature disposal, fosters a linear consumption model and significantly increases textile waste generation. Sustainable recycling solutions are thus essential for reducing textile waste, to lessen pollution and achieve a circular economy for textiles [2,5].

Recycling of textile waste is challenging due to the heterogeneous nature of the waste and the presence of contaminants from additives and dyes [4,6]. Most textiles consist of multi-material fibre compositions (e.g. cotton/polyester, cotton/polyamide 6, cotton/polyester/elastane), making the sorting and separation of these waste streams challenging and complex [4,7,8]. Sorting and separation of the fibres are necessary for mechanical and chemical recycling methods (such as dissolution), where more homogeneous streams are required [9]. The separation process, in turn, leads to fibre degradation and material losses and involves various chemicals leading to large chemical consumption and pollution. In many cases the quality of the fabrics and fibres is so poor that the recovery and re-spinning of the textile yarn is not feasible [1,6–8,10].

Thermochemical conversion is a robust and versatile technique able to convert various heterogeneous waste streams (biogenic to plastic-rich waste) to gaseous or liquid products. Thermochemical conversion

Abbreviations: ar, As received; BFB, Bubbling fluidized bed; B+T, Benzene and toluene; BTX, Benzene, toluene and xylenes; daf, Dry, ash-free basis; db, Dry basis; DME, Dimethyl ether; FID, Flame ionisation detector; FTIR, Fourier Transform Infrared Spectroscopy; GC, Gas chromatographer; ICP-MS, Inductive coupled plasma mass spectrometry; IPA, Isopropanol; MDI, Methylene diphenyl diisocyanate; MW, Molecular weight; PA6, Polyamide 6; PAH, Polycyclic aromatic hydrocarbon; PE, Polyethylene; PET, Polyethylene terephthalate; PP, Polypropylene; PUR, Polyurethane; StC, Steam-to-carbon; WGS, Water-gas-shift.

* Corresponding author.
E-mail address: surika.vanwyk@tno.nl (S. van Wyk).

https://doi.org/10.1016/j.fuel.2025.137564
Received 30 July 2025; Received in revised form 18 October 2025; Accepted 14 November 2025

includes techniques such as gasification (direct or indirect), thermal cracking and pyrolysis. The suitability of these techniques for handling various heterogeneous waste streams, such as mixed plastic waste, municipal solid waste and refuse-derived fuel, has been demonstrated in numerous studies [11–19]. During these processes, the feedstock is converted to products such as syngas (CO + H_2), hydrogen, methane, olefins (C_2H_4 and C_3H_6), benzene, toluene and xylene (BTX) and other liquid products. The products are either used for the production of new monomers/polymers to produce plastics (closed-loop recycling), or in other applications such as the production of fuels and chemicals [11,17,18].

The versatility and robustness of these techniques makes it a suitable solution to treat the larger heterogeneous textile waste streams that are not fit for other recycling methods. A few studies investigated thermochemical techniques for recycling textile waste including torrefaction, pyrolysis and gasification [6,10,20–30]. Zhuang et al. [10] studied the production of hydrogen-rich syngas through steam gasification of a real polyester-cotton waste stream under various conditions. Wen et al. [23] investigated the pyrolysis and gasification performance (under a CO_2 atmosphere) of three textile waste streams (polyester fibre, cotton and woollen). The results showed that for both gasification and pyrolysis, cotton was the most reactive, whilst CO had a high concentration in both product gases (gasification and pyrolysis).

Canete Vela et al. [20] investigated the valorisation of textile waste through steam gasification using the model components polyethylene terephthalate (PET), cotton and a PET/cotton mixture and concluded that textile waste is promising for the production of syngas and aromatics. Yasin et al. [21,22] studied gasification of flame retardant textiles (cotton) as an alternative to incineration, and showed that textile waste could be treated to produce syngas. Gracia-Monforte et al. [28] investigated the gasification of textiles waste (cotton + PET) for varying gasifying agents, concluding that steam and air enhanced syngas quality to be suitable for energy and chemical applications. Circular Economy Foundation and Biomimicry Institute published a report on a pilot study (design for transformation), which investigated a system of technologies to process mixed textile waste. The residual waste stream, left after the removal of cellulose (cotton), was processed via thermal cracking and both syngas and BTX were retrieved as the main products from the process [30].

Most studies on thermochemical conversion of textile waste have focussed only on the main building blocks of textiles, namely PET (building block of polyester) and cotton, and on PET/cotton blends using either model components of sorted fractions of textile waste. Forero-Franco et al. [29] investigated thermal cracking of three different textile waste streams (varying compositions) for varying temperatures and concluded that cotton-rich blends yield more syngas and hydrocarbons, while PET-rich blends yield more aromatics. The results were compared to references which only included PET (for the synthetic fraction) and cotton. Textiles are complex mixtures, with most post-consumer textile waste containing > 50 % synthetic fibres. These fibres comprise a wide range of polymers such as polyesters, polyamides, polyurethane, polyolefins and polyacrylics, which all influence the thermochemical behaviour and product distribution [1,31]. It is therefore important to understand the influence of these different polymers on the product gas distribution to enable further development of thermochemical processes for the effective valorisation of textile waste.

The aim of this study was to investigate the effect of different polymers (commonly present in the synthetic fraction of textiles) on the thermochemical conversion of textile waste by testing four model mixtures that are representative of this fraction. In addition, a real post-consumer textile waste stream (not sorted for specific fractions) was investigated under various conditions (temperatures and steam flows) for comparison and to evaluate the conversion behaviour. By comparing the model synthetic mixtures with real textile waste, the study aims to assess the influence of different polymers on the resulting product distribution and compare it with a real textile waste stream intended for incineration. The focus was on identifying high-value and versatile products that can be retrieved from mixed textile waste, with implications for new fibre production (closed-loop recycling), as well as chemical and fuel production. The results provide insight into the role of different polymers during the thermochemical conversion of textile waste and demonstrate the feasibility of thermochemical conversion for sustainable textile waste management.

2. Experimental

2.1. Materials

Model mixtures and real textile waste were both investigated, with the building blocks of the different synthetic fibres considered for the model mixtures. The polymers investigated were PET (building block of polyester), polyamide 6 (PA6 – also known as nylon 6) and polyurethane (PUR – building blocks of elastane/spandex). These polymers are considered the main synthetic building blocks of most textiles [1,31]. PET (polyester) is the main building block of the synthetic fraction of textiles, accounting for 84 % of the global synthetic fibre production in 2020. Polyamides and polyurethanes account for 8.1 and 1.6 % respectively, while acrylics and other synthetic fibres account for the remaining 9.7 % of the global synthetic fibre production [31]. The PET fraction was maintained between 80 – 90 % to reflect its majority presence in the synthetic fraction, while PA6 and PUR were each added at 10 % to reflect the minor (relative to polyester) contribution (see Table 2). The concentrations were not lower to ensure observable differences in the product distributions. The polymers were in the form of pure virgin plastic beads (PA6: Akulon® F136-C1 PA6 produced by Envalior, circa 3 mm beads / PUR: Ravathane® TPU produced by Ravago, circa 3 mm beads / PET: Billion PET supplied by Resinex, circa 3 mm beads). Fourier Transform Infrared Spectroscopy (FTIR) analysis of the PUR indicated that it contained a methylene diphenyl diisocyanate (MDI) structure.

The real textile waste was supplied by the Boer Group and consisted of a sorted stream of post-consumer textile waste intended for incineration. The stream contained different articles of clothing and other items such as blankets and bedding. Before the material could be fed to the reactor, it was pre-processed to enable feeding with a screw feeder. Pre-processing was done by directly shredding the textile waste followed by feeding the shredded material through a pelletizer (15 times), resulting in a dense fibrous material that could be fed with the screw feeder. No further pre-processing, such as drying, was done afterwards. The zippers, buttons and other metal parts were not removed during the feedstock preparation and could be fed to the reactor without experiencing operational challenges. The steps of the textile processing can be seen in Fig. S.1 in the supporting information (SI). The results of the proximate and elemental analysis, as well as the calorific value of the tested feedstocks, are presented in Table 1.

The ash yield of the real textile waste was the highest, owing to a higher presence of inorganics in the stream coming from fillers and additives used during the production of textiles. This was also evident from the higher concentration of contaminants, such as sulphur and chloride, in the real feedstock compared to the pure polymers. The bromide concentration, which is an indication of fire retardants, was below detection limits for the pure polymers, but was higher for the real textile waste indicating the presence of fire retardants in the waste stream. Additional inductive coupled plasma mass spectrometry (ICP-MS) analysis was performed to quantify the concentrations of metals and other trace elements in the feedstocks (see Table S.1 in the SI). The results provide further information on the contaminants from fillers, additives and chemicals used for the production of textiles. For pure polymers, the concentrations were below the detection limits for most components. For the real textile waste the concentrations of aluminium and iron were high, due to the zippers, buttons and other metal items not being removed during the feedstock preparation. The concentrations of

Table 1
Feedstock analysis results.

	Unit	PET	PUR	PA6	Real textiles
Calorific value	MJ/kg (db)[a]	21.9	25.8	29.1	20.9
Proximate analysis					
Ash (at 550 °C)	wt.% (db)	< 0.1	< 0.1	< 0.1	1.4
Moisture	wt.% (ar)[b]	< 0.1	< 0.1	< 0.1	4.6
Volatiles	wt.% (db)	93.7	98.1	100.3	88.2
Elemental analysis					
C	wt.% (db)	62.4	63.1	62.4	54.8
H	wt.% (db)	4.3	7.0	9.8	5.6
N	wt.% (db)	0.0	3.9	12.0	1.8
O[c]	wt.% (db)	33.2	25.9	16.2	32.2
S	mg/kg (db)	< 25	< 25	< 25	726
Cl	mg/kg (db)	27.7	17.0	23.3	546
Br	mg/kg (db)	< 10	< 10	< 10	34.1
F	mg/kg (db)	< 10	< 10	< 10	< 10

[a] db – dry basis.
[b] ar – as received basis.
[c] directly measured, not calculated by difference.

calcium, magnesium, silicon and titanium were also higher. Titanium (used as titanium-silver nanoparticles) is used for ultraviolet protection and antimicrobial, while calcium is used as a filler in the form of calcium carbonate and calcium sulphate. Magnesium is used as a dye fixative to ensure that dyes adhere properly to the fibres for long lasting colours, while silicones are used to increase softness and flexibility, as well as oil and water resistance and for improved durability [32]. The oxygen content of the real textile waste was similar to PET, however the oxygen contribution for the real textile waste comes from both the synthetic fraction (from polymers such as PET, PA6 and PUR) and the biogenic fraction (such as cotton and wool). The exact polymer composition of the real textile waste stream was not known, but the glucan content was determined via hydrolysis to have an indication of the biogenic content, which mainly consists of cotton fibres and to a lesser extent wool and silk. Based on the glucan content, the biogenic concentration was ±58 wt%, which was assumed to be mainly cotton in this study.

2.2. Experimental set-up and procedure

Experiments were performed in the multi-purpose bubbling fluidized bed (BFB) reactor located at the TNO site in Petten, The Netherlands. A basic schematic of the installation and the gas analysis train is given in Fig. 1.

The reactor consisted of two zones, the bottom zone where the bed was located and the top zone, namely the freeboard. The inner diameter and height of the bottom zone was 74 and 500 mm respectively, while for the freeboard it was 108 and 600 mm. The reactor was operated under atmospheric pressure and was traced with heating elements at the wall, to provide external electrical heating (maximum operating temperature of 1100 °C). Fluidization gases such as N_2, air and/or steam were introduced in the bottom of the reactor. The solid feedstock was fed directly into the fluidized bed via a screw feeder which was calibrated

Table 2
Experimental conditions for the different feedstock tests.

Parameter	Unit	Run 1	Run 2	Run 3	Run 4	Run 5	Run 6	Run 7	Run 8	Run 9
Feedstock[a]		100 % PET	90 % PET + 10 % PUR	90 % PET + 10 % PA6	80 % PET + 10 % PUR + 10 % PA6	Real textiles	Real textiles	Real textiles	Real textiles	Real textiles
Duration of run	min	45	47	53	115	64	76	161	131	119
Average reaction temperature	°C	706	706	706	707	707	755	802	853	853
Feed rate	g/h (ar)[b]	358	426	409	382	239	239	147	143	143
N_2 flow[c]	NL/min	9	9	9	9	10	10	9	9	11
Steam flow	g/h	180	196	200	200	110	110	70	70	0
Steam/carbon ratio[d]	g/g	0.81	0.80	0.78	0.94	0.97	0.97	1.00	1.03	0.09[e]

[a] Fraction of synthetic mixtures are based on weight (wt.%).
[b] On as received (ar) basis.
[c] Including the 1 NL/min N_2 on the feeding screw.
[d] Includes the moisture of the feedstock.
[e] Steam/carbon ratio is not zero due to moisture in the feedstock.

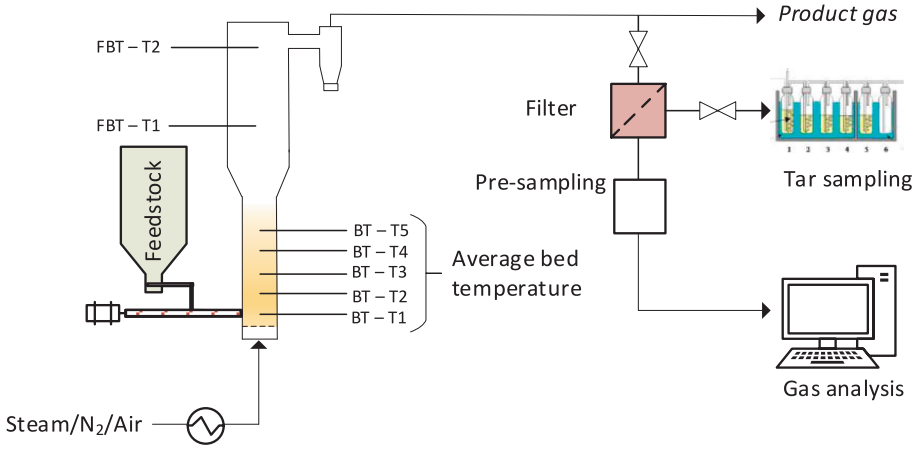

Fig. 1. Schematic of the bubbling fluidized bed installation with analysis. (BT – Bed temperature; FBT – Freeboard temperature).

beforehand for the desired flow rate (maximum feeding capacity was 500 g/h). The feeding bunkers were weighed before and after each experiment to determine the average feeding rate over the experimental time. The reactor was equipped with K-type thermocouples, located at various positions in the bed and freeboard, to verify that the temperature distribution was even throughout the reactor. In addition to the thermocouples, the reactor was equipped with various pressure sensors to monitor the pressures and fluidization behaviour of the bed inside the reactor.

For the experiments, the reactor was filled with 1.3 kg quartz sand (dp_{50} = 310 μm; sieved to remove fines < 250 μm; Dorsilit® 9 Cristal quartz sand (94 % SiO_2) supplied by Dorfner), and steam and N_2 were used as fluidization mediums. The steam flow was adjusted so that the steam-to-carbon (StC) ratio was 0.8 (g/g) and additional N_2 was added to ensure operation at five times the minimum fluidization velocity. The required minimum fluidization velocity was calculated prior to each test to ensure proper hydrodynamics and to ensure that the conditions were comparable for each experiment. A few tests were performed in the absence of steam and only N_2 was fed to the bottom of the reactor. Neon (20 NmL/min) was added to the bottom of the reactor (with the fluidization gases) as a tracer gas, to determine the volumetric product gas flow rate. The product gas was sampled and measured (online and offline) at the outlet of the reactor for the quantification of the products (See Section 2.3). Prior to each experiment the reactor was heated to the desired temperature and N_2 and/or steam was introduced to fluidize the bed. To prevent the backflow of hot gases from the reactor to the feeding screw, 1 NL/min of N_2 was added to the feeding screw.

Once stable conditions were reached, the feedstock (pulverized textile material – see Fig. S.1 in the SI) was introduced via the feeding screw and the N_2 flow was reduced as it was substituted by the product gas being formed. In the SI the fluidized bed temperature profiles (Figs. S.2 and S.3), of a test with a model mixture and a test with real textile waste, are given along with the concentration profiles (Figs. S.4 and S.5) of the permanent gases. The offline samples, namely the gas bags and wet chemical samples, were taken 10 – 15 min after steady state was reached to ensure that conditions were stable and the results would be representative. All offline samples were taken twice, and the average of the results are presented in this study. Upon completion of the experiment, the feeding and steam (and/or N_2) were stopped, and air was introduced into the bed to combust the residual carbon. The CO_2 and CO concentration was measured at the outlet of the reactor and used to quantify the residual carbon material remaining in the bed after the experiment. In Table 2, the experimental conditions for the tests are summarized. The feed rate of the real textile waste was lower compared to the synthetic mixtures due to the low density of the material (pulverised material) compared to the high density of the virgin beads. For this reason, the N_2 flow rate was increased for run 5 and 6 to ensure that the hydrodynamics and residence times were comparable for each run. For run 7 and 8, the flow rate of N_2 was lower due to higher product gas yields achieved at higher temperatures. For run 9, only N_2 was used as fluidization medium (no external steam was added) and thus the flow rate was higher. The reaction temperature for the model synthetic mixtures were set to 700 °C, which is within the preferred temperature range for plastics thermal cracking for the retrieval of gaseous products (olefins) and aromatics. For the real textile waste streams, the temperature was increased to 850 °C in steps of 50 °C to investigate syngas production.

2.3. Analysis

The product gas exiting the top of the reactor was analysed using both online and offline analysers. Continuous online measurement of the permanent gases (CO, CO_2, CH_4, H_2 and O_2) was done with an ABB gas analyser. A Varian micro-gas chromatographer (GC) analyser, which analysed the product gas (N_2, Ne, Ar/O_2, CO, CO_2, CH_4, C_2H_2, C_2H_4, C_2H_6, C_3H_6, C_3H_8, benzene, toluene H_2S and COS) at six-minute intervals, was also connected and used for online measurements (relative error of 2–5 %). Gas bags were taken during steady-state operation and analysed offline with a Thermo Scientific Trace 1310 GC with a flame ionisation detector (GC-FID) to quantify the C_1-C_6 hydrocarbons, as well as H_2 (relative error of 2–5 %). Lastly, wet chemical sampling (in isopropanol (IPA)) of the gas was done according to the standardised tar measurement protocol to quantify the tar components (molecular weight (MW) > 78 g/mol) as well as benzene and toluene [33]. For biomass and biogenic feedstocks, the sampling time of the tar measurement is normally 30 min, however for plastic feedstocks the tar yields are higher and thus the sampling time was reduced to 15 min to avoid oversaturation of the IPA solution and breakthrough of components such as benzene and toluene [34]. The samples were analysed afterwards using GC-FID to measure the polycyclic aromatic hydrocarbons (PAHs). During combustion of the residual carbon, after the experiment, the online analyser was used to measure the CO_2 and CO concentrations for solid carbon quantification.

The NH_3 and HCN concentrations in the product gas were measured via impinger sampling followed by offline analysis of the samples. For the NH_3 analysis, the gas was sampled using two impingers in series (placed in a cool batch at 4 °C) containing 0.1 M HNO_3 solution. For HCN, the two impingers were filled with a 2.5 M NaOH solution. The NH_3 sample was analysed by ammonia flow injection analysis, while the HCN sample was sent for external analysis. More details on the sampling and analysis methods are provided in [35]. The model mixture gases were not sampled as the concentration of the nitrogen containing polymers were low (only 10 % of the mixture). Only the product gas of real textile waste was sampled (runs 7 – 9, see Table 2).

2.4. Product yield and carbon balance

The results of the product gas flow, along with the measured concentrations of the individual species, were used to calculate the volume flow of each component ($\dot{V}_i$ in NL/h). Next, the carbon flow of each component ($\dot{C}_i$ in g_{carbon}/h) was calculated from the volume flow, as shown in Eq. (1).

$$\dot{C}_i = \frac{\dot{V}_i}{22.414} \times MW_i \times c_i \tag{1}$$

where MW_i is the molecular weight of component i(g/mol) and c_i is number of carbon atoms present in the molecule of species i. The carbon yield of each component ($Y_{carbon,i}$(%)) was calculated based on the carbon flow of the feedstock ($\dot{C}_{feedstock}$ in g_{carbon}/h), as shown in Eq. (2).

$$Y_{carbon,i} = \frac{\dot{C}_i}{\dot{C}_{feedstock}} \times 100 \tag{2}$$

The carbon balance for each experimental run was calculated by dividing the carbon exiting the system (product gas, aromatics and solid carbon) by the carbon entering the system (from the feedstock), as shown in Eq. (3)

$$Carbonclosure = \left(\frac{\sum_i \dot{C}_{i,productgas} + \sum_i \dot{C}_{i,tar} + \dot{C}_{benzene\&toluene} + \dot{C}_{solidcarbon}}{\dot{C}_{feedstock}} \right) \times 100 \tag{3}$$

The hydrogen and oxygen yields were calculated in a similar manner as described in Eq. (1) & (2). Instead of multiplying with the c_i, the multiplication was done with either the number of hydrogen or oxygen atoms in the molecule of species i to get the hydrogen and oxygen mass flows, respectively. The hydrogen and oxygen yields were calculated based on the hydrogen and oxygen in the feedstock only, not the total hydrogen or oxygen entering the system which includes the steam. This

approach assists with determining the extent of feedstock devolatilization and cracking to release hydrogen and oxygen, while also evaluating steam participation in the reactions. The errors for the yields were calculated with the error propagation method, using the uncertainties in the product gas flow, feed rate of feedstock and measured concentrations of the components.

3. Results and discussion

3.1. Comparison of feedstocks

The mass yields of the different products (non-condensable gas, aromatics and solids) were calculated based on the feedstock flow rate (on a dry-ash free (daf) basis). The mass yields are presented along with the H_2 and carbon yields in Fig. 2a and b for the model mixtures and real

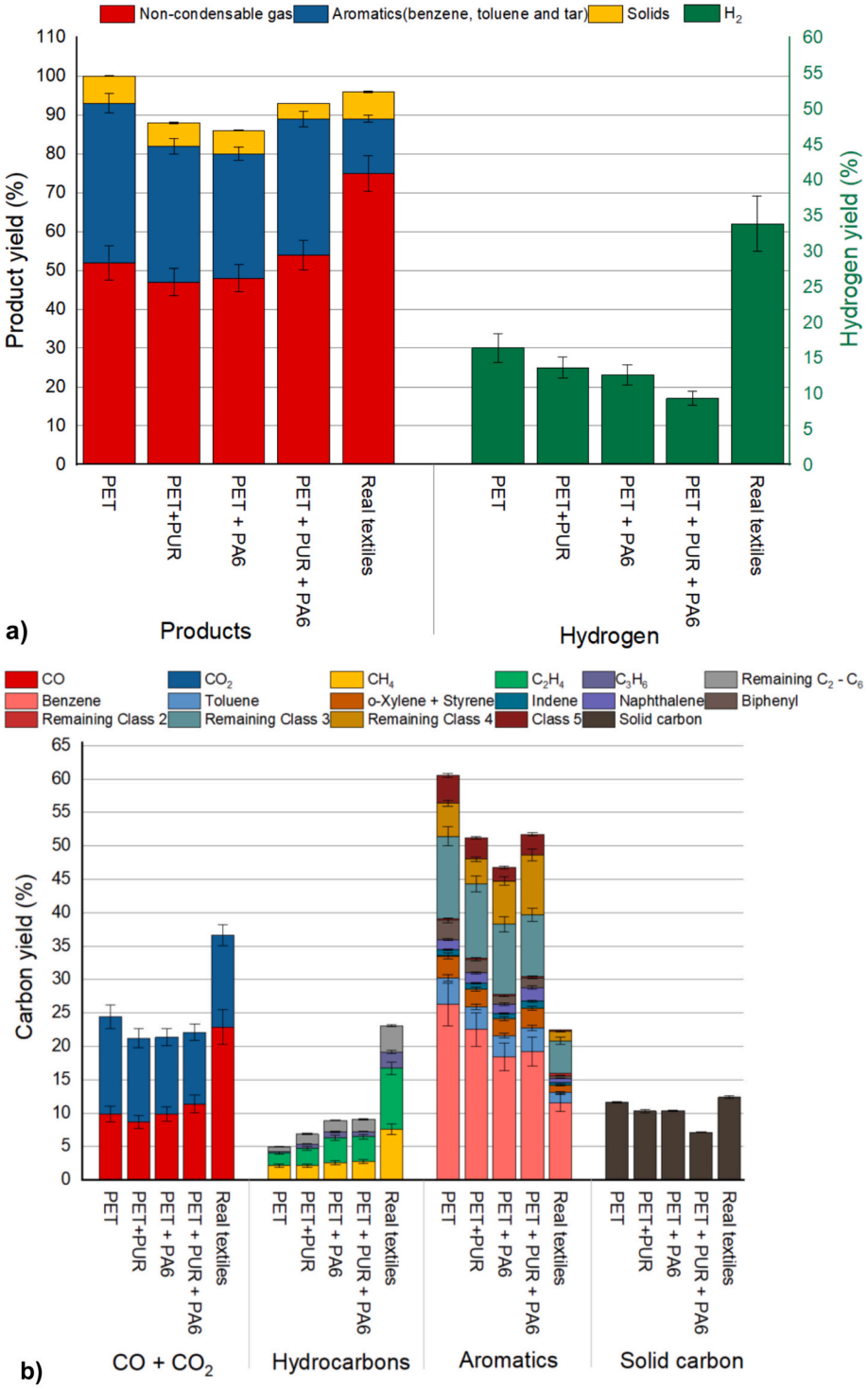

Fig. 2. Comparison of mass yields for the model mixtures and real textile waste at 700 °C and StC 0.8 a) Main product mass yields based on the feedstock mass (daf basis) and H_2 yields in the product gas based on the hydrogen content of the feedstock. b) Carbon yields of products based on carbon content of the feedstock (Error bars calculated using the error propagation method).

textile waste (700 °C and StC of 0.8). The remaining tar components not specifically mentioned in Fig. 2b were grouped together according to the tar classification described in [36]. Class 2 tar components refer to heterocyclic aromatics, class 3 refers to 1 ring aromatics, class 4 to 2 & 3 ring PAHs and class 5 to 4 & 5 ring PAHs. The carbon yields along with the calculated hydrogen and oxygen yields for each species are presented in Tables S.2–S.4 in the SI.

The largest uncertainty for the yield error calculation was the uncertainty in the feed rate, which was 10 %. The uncertainties in the product flow rate and gas phase concentrations were <5 %. The solids' yields were comparable for all feedstocks ranging between 6 and 7 %, with the exception of PET + PA6 + PUR mixture, where it dropped to 4 %. The solids in the bed, which was assumed to be mainly carbon, was due to the formation of soot (from thermal cracking of polymers) and heavy tar components depositing in the bed. As shown in Table 1, the volatile content of the polymers was between 94 and 100 wt%, indicating that minimal char was produced (fixed carbon was low). For the four model mixtures, the non-condensable product gas and aromatics yields were comparable, owing to the mixtures, mainly consisting of PET (≥80 wt%).

Syngas (CO and H_2) and CO_2 were the main components contributing to the product gas yield for the model mixtures. The results correspond with previous studies reporting similar product gas compositions and evaluating the product distribution for the thermal degradation of PET, PUR and PA6 [13,37–39]. Li et al. [40] reported that steam gasification of PET predominantly produced CO_2, with a carbon yield of ±8 % for CO and ±16 % for CO_2 at 700 °C. Forero-Franco et al. [29] reported carbon yields of ±9 % for CO and ±14 % for CO_2 at 760 °C, while for this study the yields were 10 % for CO and 15 % of CO_2. Cantele Vela et al. [20] also reported CO_2 as the predominant gas phase product during the steam gasification of PET, along with elevated tar yields (including benzene). The high CO_2 and aromatics yield associated with PET is mainly ascribed to the thermal decomposition of PET, with minimal contribution of steam for steam reforming reactions and the subsequent water–gas-shift (WGS) reaction to produce CO_2. PET is composed of benzene rings, ethylene glycol and two ester linkages and has a high fraction of aromatic carbon bond groups (carbons attached to aromatics) in the structure [29]. At elevated temperatures PET decomposes to terephthalic acid, which in turn decomposes to benzoic acid while releasing CO_2 (via decarboxylation). As the temperature increases benzoic acid decomposes to benzene and biphenyl, simultaneously releasing CO_2 through the breakdown of the ester/carboxyl groups [40–42]. CO (and CH_4) are produced to a lesser extent through the breakage of aldehydes, formed by the partial hydrolysis of esters and subsequent alcohol oxidation [42,43]. From the oxygen balance, 73 % of the oxygen in the feedstock is converted to CO_2, while 25 % is converted to CO. The oxygen balance closure was 98 %, based on the oxygen in the feedstock only, indicating that steam contributed minimally to CO and CO_2 formation. Benzoic acid was not quantified as it was not part of the analytical scope of this study. At 700 °C, the oxygen balance closure for PET was close to 100 %, with the majority of the oxygen in the feedstock going to the gas phase, suggesting that the yields for benzoic acid and other unaccounted oxygenated tar components were low.

As the PET concentration in the mixture decreased, with the addition of PUR and PA6, the yield of CO_2 and other decomposition products namely benzene and biphenyl decreased due to reduced thermal decomposition of PET. The decrease in these yields led to an overall reduction in the aromatics carbon yield of the mixtures containing PUR and PA6. PUR and PA6 have complex polymer structures and thermal decomposition leads to a multitude of products (aromatics, gases, solids) [44–47]. At higher temperatures (> 600 °C) gas and tar are the major products for PUR thermal degradation, with CO as the major gas-phase component followed by CH_4 and C_2H_4 [38,44,48]. The carbon yields in Fig. 2b show that the hydrocarbons yield, mainly C_2H_4 and remaining C_2 – C_6, increased with the addition of PUR, which was attributed to dehydrogenation and deamination of alcohols and amines (decomposition products of MDI-based PUR). Syngas and NH_3 are produced in parallel, together with CO_2 during hydrolysis of isocyanates [44,46]. The CO + CO_2 and H_2 yield dropped with the addition of PUR, indicating lower production of these components compared to pure PET. The drop in yields also indicates a minimal effect of steam in steam reforming and WGS at this temperature range. Steam reforming reactions are endothermic and have a limited extent at lower temperatures [49]. The limited effect of steam can also be seen from the oxygen and hydrogen balances, where the balance closures were below 100 %.

With the addition of PA6 to PET, the hydrocarbons yield increased further due to PA6 being an aliphatic polyamide, with a large fraction of the polymer consisting of aliphatic carbon bond groups (carbon attached to aliphatics) [50,51]. During thermal decomposition, the polymer chains undergo scission that releases free radicals which propagate further degradation of the polymer, generating additional radicals. These radicals react to form smaller hydrocarbons (e.g. CH_4, C_2H_4 and C_3H_6), as well as nitrogen containing components such as nitriles (from amide dehydration) [12,48,50,52]. The CH_4 and C_2H_4 showed the largest increase as these are more stable, compared to hydrocarbons such as C_3H_6 and C_4H_8 which more readily undergo secondary reactions [53,54]. The overall CO + CO_2 yield remained constant with a small shift towards higher CO and lower CO_2 yields. CO and CO_2 are both produced during the thermal degradation of caprolactam (from the degradation of PA6), with studies indicating that CO formation is favoured over CO_2 at higher temperatures [13,55]. The higher yield is also attributed to CO not being consumed during the WGS reaction under these conditions. The oxygen and hydrogen balances closures did not exceed 100 %, once more indicating the limited effect of steam for these conditions. The overall aromatics carbon yield decreased with the addition of PA6, however, the remaining class 4 tar yield increased, which is due to the degradation products of caprolactam [47,55].

PUR and PA6 are both nitrogen containing polymers, with NH_3 and HCN forming part of the product gas composition, however the measurement of the nitrogen containing species was not within the analysis scope of this study for the model synthetic mixtures. The NH_3 and HCN concentration in the product gas of the real textiles waste was measured for runs 7 – 9 to have a first indication of the concentrations present in the product gas of real textile waste (refer to Section 3.2.3).

For the PET + PUR + PA6 mixture, the hydrocarbons yield once more increased compared to pure PET, mainly due to thermal degradation of PA6. The aromatics yield also increased due to the increase in indene, naphthalene and remaining class 4 aromatics yield. The observed increase in class 4 aromatics yield is attributed to the addition of PA6, while the increase in indene and naphthalene is presumed to result from possible interactions between the products obtained during thermal cracking. The increase in yields were not observed for PUR and PA6 respectively. From the overall oxygen balance closure, it is seen that the closure decreased to 86–88 % with the addition of PA6 and PUR, indicating that not all oxygen containing species were accounted for. These species could include polyols, isocyanate and caprolactam and water, which are degradation products of PUR and PA6, but were not part of the analytical scope of the study [44–47,55].

For the real textile waste, a significant shift in the distribution of non-condensable gas and aromatics yields was observed when compared to the model mixtures, with the gas yield increasing to 75 % and the aromatics yield decreasing to 14 %. The shift in distribution is assumed to be due to the cotton fraction of the real textile waste and the presence of other polymers that are typically found in textile waste (such as polypropylene (PP) and poly acrylic nitrile (PAN)) alongside PET, PUR and PA6 [1,29].

The CO yield, for the real textile waste, increased compared to PET and PET mixtures which favoured CO_2 formation. Although the real textile waste stream and PET had similar oxygen content (see Table 1), the chemical structure of PET vs. cellulose plays a crucial role in the product distribution for thermal cracking [51]. PET composed of terephthalic acid (contains benzene rings) and ethylene glycol linked with

ester bonds, primarily produce carboxylic acids and vinyl esters during thermal degradation. The carboxylic acids undergo decarboxylation forming CO_2 and aromatics such as benzene, leading to the high yields of CO_2 and aromatics seen in Fig. 2b. CO is also formed via the decomposition of aldehydes, however the yields are comparatively lower [42]. In contrast, cotton (cellulose) consists of linear polysaccharides with glucose units linked by glycosidic bonds formed by the hydroxyl groups condensation, creating oxygen bridges between the units [29,56]. The thermal degradation of cellulose produces CO and CO_2 via radical pathways including cleavage, isomerization, binding to oxygenated radicals, hydrogen abstraction and oxidation [57,58]. Wei et al [57] reported that CO formation is favoured over CO_2 formation due to its various generation pathways and lower energy barriers. Canete Vela et al. [20] showed increased CO concentrations for both pure cotton and blended feedstocks, compared to that of pure PET. Other studies also showed higher yields of CO_2 (relative to CO) for PET than for the cellulose streams under similar conditions [25,39,59].

In addition to CO and CO_2, H_2 and CH_4 are major gaseous products of cellulose gasification. CH_4 is formed via methyl radicals released during cracking, while H_2 is produced during dehydrogenation and cracking of hydrocarbons and tar, leading to higher CH_4 and H_2 yields compared to PET [29,58,59]. Apart from CH_4, C_2H_4 (formed from acrolein via vinyl radicals) has a notable concentration in cellulose derived gas mixtures [29,58]. Cellulose contains more aliphatic carbon bond groups (compared to PET), which undergo cracking reactions to form smaller hydrocarbons. Thermal degradation of PET also yields C_2H_4, via end-chain cleavage, however the yields are lower compared to cellulose [29,60]. In addition to higher CH_4 and C_2H_4 yields, Forero-Franco et al.

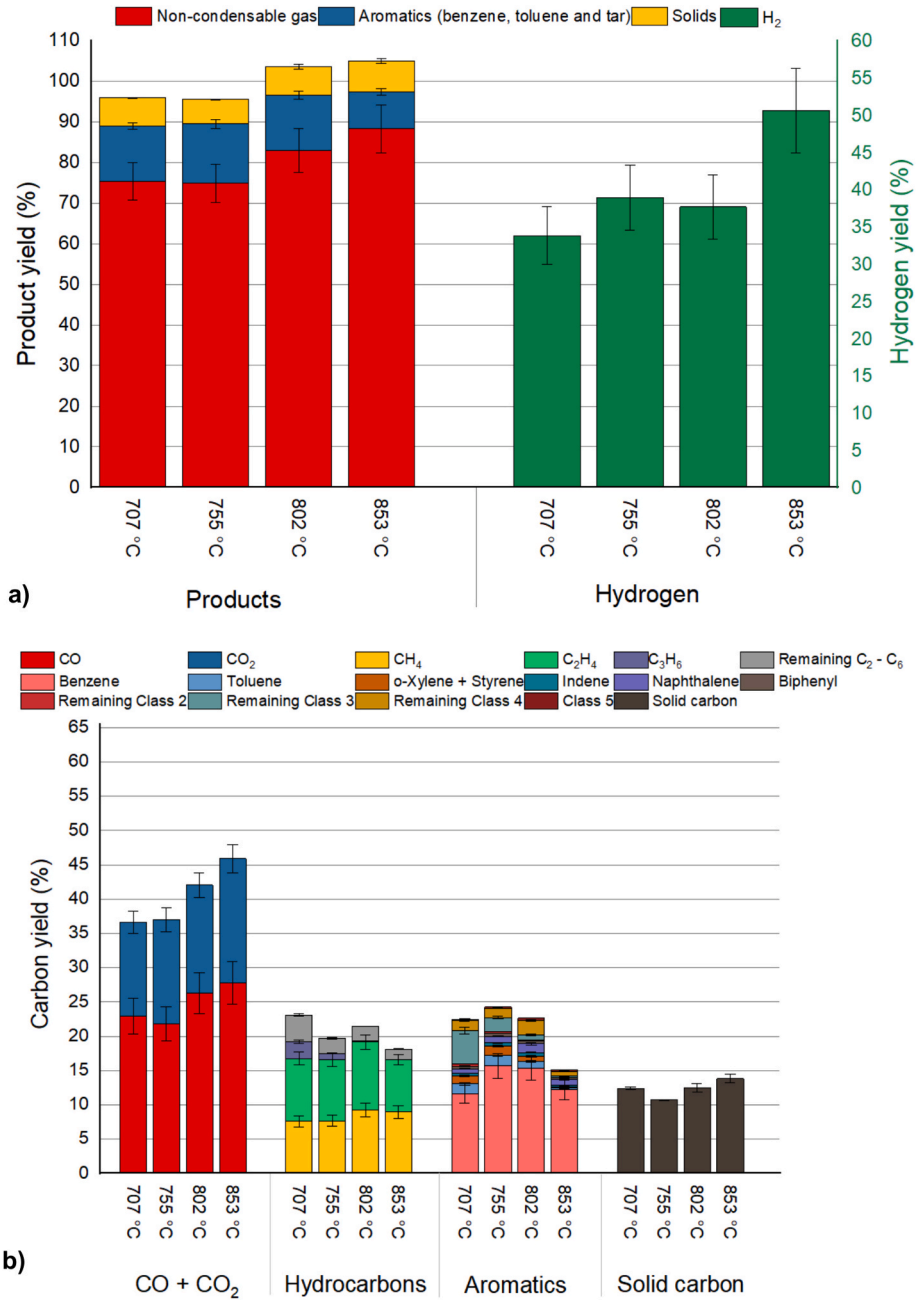

Fig. 3. Comparison of yields for the real textile waste at different temperatures and StC 0.8 a) Main product mass yields based on the feedstock mass (daf basis) and H_2 yields in the product gas based on the hydrogen content of the feedstock. b) Carbon yields of products based on carbon content of the feedstock (Error bars calculated using the error propagation method).

[29] reported higher carbon yields for hydrocarbons such as C_3H_6 and C_2H_6 from cotton thermal cracking compared to PET, indicating an overall higher hydrocarbons yield for pure cotton compared to pure PET. Conversely, the aromatics yield of cellulose thermal cracking/steam gasification are comparatively lower, leading to an overall decrease in the aromatics yield seen in Fig. 2b [20,25,28,29,61,62]. In addition to the contribution from the cotton fraction, PP and PAN, potentially present in the real textile waste stream, contribute to higher hydrocarbons and H_2 yields compared to the synthetic model mixtures which yielded more aromatics. These polymers consist predominantly of aliphatic carbon bond groups, which thermally degrade at elevated temperatures to produce small hydrocarbons and H_2 [29,54].

3.2. Real mixed textile waste

3.2.1. Effect of temperature

In Fig. 3a and b, the product mass yields of real textile waste for different temperatures are compared along with the H_2 and carbon yields.

Increasing the operating temperature led to higher product gas yields due to the increased thermal decomposition and steam reforming of larger tar components to gaseous molecules [34,57,63,64]. For the product gas, the highest yields were seen for syngas and CO_2. Between 707 and 802 °C, the syngas yields were comparable, while at 853 °C the H_2 yield increased to 51 %. The CO_2 yield increased due to thermal decomposition of the textile waste components such as PET and the WGS reaction. The yields of C_3H_6 and the remaining $C_2 - C_6$ hydrocarbons decreased with temperature due to the promotion of secondary reactions at elevated temperatures. During secondary reactions, the larger hydrocarbons undergo further thermal decomposition to produce smaller hydrocarbons (such as CH_4 and C_2H_4) and aromatization reactions such as Diels-Alder and/or dehydrogenation to produce benzene and other aromatics. Furthermore, hydrocarbons undergo steam reforming reactions to produce syngas, which favour higher temperatures due to the endothermic nature of the reactions [49,51,54]. The yields of CH_4 and C_2H_4 reached a maximum between 755 and 802 °C, after which the yield of C_2H_4 decreased owing to further thermal decomposition to form CH_4 (via radical recombination and hydrogen abstraction) and steam reforming to produce syngas [65,66].

The shift in hydrocarbons yield coincided with an increased benzene yield at 755 °C, indicating the occurrence of secondary aromatization reactions with increased temperatures. At 755 °C the aromatics yield increased, mainly due to the increase in benzene yields and to a lesser extent the yields of other lower molecular weight aromatics (e.g. xylene, styrene and indene). At higher temperatures (802 °C), benzene reacts further to form PAHs, such as naphthalene primarily, via the hydrogen abstraction-acetylene addition mechanism which produces H_2 as a by-product, further increasing the H_2 yield. The yields of toluene and styrene also decreased with increased temperatures as these single-ring compounds serve as precursors for PAHs [62]. Even though the yields of the larger PAHs (naphthalene and class 4 PAHs) increased (up to 802 °C), the overall yield of the aromatics decreased with temperature in favour of higher solid carbon and syngas yields.

Between 707 and 755 °C, the yield of solid carbon decreased as the carbon reacted with steam to produce syngas. The reaction is endothermic, having a greater extent at higher temperatures. As the temperature increased (> 755 °C), re-polymerization of larger PAHs to form solid carbon becomes dominant over the reaction with steam, resulting in a marginal overall increase in solid carbon yield [12,51].

Fig. 3a and b shows that H_2, CO and CO_2 had the highest yields which increased with temperature. The yields increased through intensified thermal decomposition and re-polymerization of larger PAHs at higher temperatures, but also increased participation of steam through steam reforming of hydrocarbons and PAHs, as well as the WGS reaction. The hydrogen and oxygen balance closures (in Tables S.3 and S.4) exceeded 100 % for real textile waste streams, with the values rising as temperature increased. The carbon balance closure remained constant. This indicates increased steam participation at higher temperatures, which contributed additional hydrogen and oxygen to the products resulting in closures greater than 100 %. For the oxygen balance, the increase in CO and CO_2 yields contributed to the balance exceeding 100 %, while for the hydrogen balance it was due to the increase in H_2 yields. Steam reforming of hydrocarbons (and PAHs) produce H_2 and CO and are endothermic reactions favoured at higher temperatures. The occurrence of steam reforming is evident from the decrease in the hydrocarbons and PAHs yields combined with the simultaneous increase in the CO and H_2 yields. CO_2 is formed via the consumption of CO and steam, through the WGS reaction. However, the reaction is exothermic with the extent of the WGS becoming thermodynamically limited at higher temperatures. At 755 °C the CO yield decreased, with the simultaneous increase in the CO_2 yield. This suggests that the consumption of CO in the WGS reactions exceeded its formation via steam reforming under these conditions. As the temperature increased further, the CO yields showed a net increase, suggesting that the CO production exceeded the consumption due to the extent of the WGS reaction becoming limited and the enhanced contribution of steam reforming at higher temperature. The H_2 yield increased with temperature as it is a product of both steam reforming and the WGS reaction. Both the studies of Canete Vela et al. [20] and Zhuang et al. [10] showed sharp increases in H_2 yield with temperature in the presence of steam, which was attributed to enhanced steam reforming at higher temperatures. Forero-Franco et al. [29] also observed an increase in the carbon oxides yield for textile waste with temperature, which was attributed to steam reforming and WGS reactions.

3.2.2. Effect of steam

The overall product yields as well as the H_2 and carbon yields of real textile waste, for different steam flows at 853 °C, are presented in Fig. 4a and b.

As shown in Section 3.2.1, tar components undergo steam reforming reactions to produce syngas, while the solid carbon in the bed reacts with steam to produce syngas at elevated temperatures. This aligns with the observed increase in total product gas yield, with the addition of steam and subsequent decrease of the tar and solid carbon yield. The CO_2 and H_2 yield increased significantly, due to the participation of steam in the reactions as reflected by the hydrogen and oxygen balance closures exceeding 100 % for StC 1.03 (Tables S.3 and S.4). Gracia-Monforte et al. [28] showed that the addition of steam improved the syngas quality by increasing the H_2/CO ratio for textile gasification.

In the absence of steam, thermal degradation of cotton and synthetic fibres are dominant in the production of product gas, with cotton mainly yielding CO and H_2, and PET mainly yielding CO_2 and aromatics (see Section 3.1). The cotton fraction of the real textile waste was ±58 wt%, which is reflected in the product gas having a higher CO yield compared to CO_2. Fig. 4b shows that the CO yield remained constant with the addition of steam, while the CO_2 yield increased with 9 %. Even though the WGS is an exothermic reaction and typically favours the reverse reaction at higher temperatures, the presence of excess steam can shift the equilibrium forward, promoting the formation of CO_2 and H_2. The constant CO yield indicates that the production during steam reforming was equal to the consumption of CO during the WGS reaction.

The hydrocarbons yield decreased with the addition of steam, primarily due to reduced C_2H_4 and CH_4 yields which were consumed in the steam reforming reactions. The overall aromatics yield declined, more notably compared to the hydrocarbons yield, as the larger PAHs also underwent steam reforming. While the benzene and toluene yield decreased marginally (benzene showed the lowest relative decrease) with the addition of steam, the larger PAHs yields showed the most significant relative decrease. In the presence of steam smaller PAHs are formed as intermediates (from the larger PAHs), which are subsequently converted to syngas. For example, naphthalene undergoes a substitution reaction with steam to form naphthol, which is subsequently converted

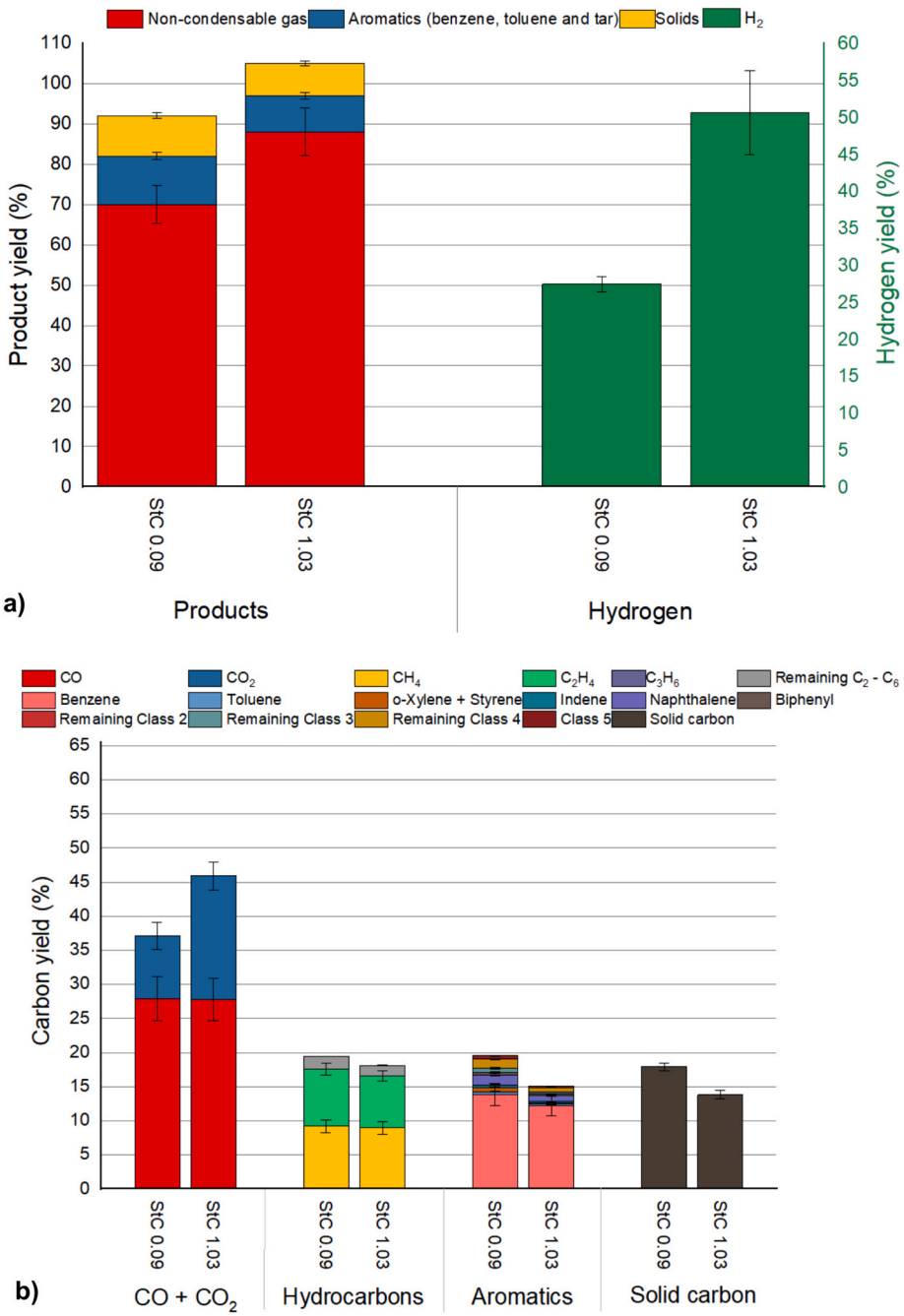

Fig. 4. Comparison of yields for the real textile waste for different steam flows at 853 °C a) Main product mass yields based on the feedstock mass (daf basis) and H_2 yields in the product gas based on the hydrogen content of the feedstock. b) Carbon yields of products based on carbon content of the feedstock (Error bars calculated using the error propagation method).

to indene via a naphthoxy radical intermediate through ring cleavage. Benzene is then formed from indene through the stepwise elimination of carbon atoms [64]. Consequently, the lighter aromatic yields (e.g. benzene) decreased comparatively less than the yields of the heavier components as they were both produced and consumed.

3.2.3. *Contaminants*

The concentrations and yields of the NH_3, HCN and H_2S in the product gas for runs 7 – 9 (see Table 2) with real mixed textile waste are presented in Table 3.

In the presence of steam, NH_3 and HCN in the product gas account for 50 – 70 % of the nitrogen introduced via the feedstock. The remaining nitrogen from the feedstock was presumed to be present in the form of nitriles, isocyanates (e.g. phenyl isocyanate), amino compounds and heterocyclic nitrogen species (e.g. pyrrole and pyridine) or remained in the char where it formed NOx upon subsequent combustion of the residual carbon in the bed after the experiment [38,44,46,48]. For increased temperatures, the NH_3 concentration (and yield) increased due to amines (released during the thermal decomposition and hydrolysis of PUR) undergoing deamination to form NH_3 and the phenyl isocyanate reacting with steam to form NH_3 [44,46]. NH_3 is also formed during the thermal decomposition of caprolactam at elevated temperatures [45]. During the thermal decomposition of PUR, HCN is formed via isocyanate cleavage, nitrile formation and aromatics ring scission (of e.g. benzonitrile), but undergoes hydrolysis reactions to form NH_3 and CO, with the reaction being promoted at higher temperatures [44,67]. This is

Table 3
Concentration and yield of NH_3, HCN and H_2S for real textile waste[a].

	Unit	802 °C	853 °C	853 °C – no steam
NH_3	ppmV (%m/$m_{nitrogen}$)[b]	9,964 ± 86[d] (34.4 ± 3.5[e])	15,549 ± 46 (60.5 ± 6.1)	5,774 ± 192 (17.2 ± 1.8)
HCN	ppmV (%m/$m_{nitrogen}$)[b]	3,026 ± 53 (10.5 ± 1.1)	2,460 ± 74 (9.6 ± 1.1)	4,436 ± 16 (13.2 ± 1.3)
H_2S	ppmV (%m/$m_{sulphur}$)[c]	302 ± 33 (0.6 ± 0.09)	265 ± 19 (0.6 ± 0.07)	b.d[f] (–)

[a] All concentrations are on a N_2-free dry, tar-free basis.
[b] Yield calculated based on the nitrogen content in the feedstock.
[c] Yield calculated based on the sulphur content in the feedstock.
[d] Error based on standard deviation.
[e] Error based on error propogation.
[f] Below detection limit (10 ppmV).

reflected in the marginal decrease in HCN yield with the increasing temperature, and simultaneous increase in NH_3 concentration. In the absence of steam (at 850 °C) the HCN increased as it was not converted to NH_3 via hydrolysis. The combined yield of HCN and NH_3 decreased to ±30 % of the feedstock nitrogen content, and it is presumed that the yields of amines, isocyanate and nitriles increased, as these species were not converted to NH_3 in the absence of steam.

For H_2S, the concentrations (and yields) were low and remained constant with the increase in temperature. In the study of Gracia-Monforte et al. [28], the H_2S concentration in the syngas was also low, despite the sulphur concentration in the feedstock being higher than the textile waste for this study. The majority of the sulphur is presumed to remain in the ash and char, as the sulphur in the textile waste is primarily derived from dyes and fillers used during the production of textiles (in the form of sulphates) which are not easily volatilized. Morrin et al. [68] stated that sulphur species are predominantly retained in the solid phase as alkali and transition metal sulphide (rather than H_2S in the gas phase) when the feedstock contains notable concentration of sodium and potassium, which was measured for the textile waste stream of this study (see Table S.1 in the SI). In the absence of steam the concentration dropped to below the detection limit of the analysis, which is assumed to be due to the decrease in H radicals (from steam) which promotes the formation of H_2S via hydrogenation of organic sulphur compounds [67].

4. Opportunities and challenges

From Section 3, it is seen that various products were retrieved for model mixtures and real textile streams under different conditions. The main product yields (based on total feedstock fed) for real textile waste are presented in Table 4.

Syngas was the predominant product, accounting for 30 – 40 wt% of the feedstock. Next to syngas, benzene + toluene (B + T) had the highest yield. From the comparison with the model mixtures (Section 3.1) it was seen that the yields of B + T were higher, which would indicate that as the polyester fraction in the textile waste increases, the yields of B + T would also increase. Forero-Franco et al. [29] reported syngas yields between 12 – 18 wt% (735 – 815 °C) for thermal cracking, while the BTXS fraction accounted for 10 – 13 wt%. The difference in yields is attributed to the higher PET fraction (> 60 %) in their waste streams, compared to this study. Nevertheless, syngas and aromatics were still the main products in both studies. Other studies have also identified syngas as the main product of gasification and thermal cracking of textile waste, particularly cotton-rich textiles, while aromatics are reported as a major product for polyester-rich textiles [10,20–22,28].

Table 4
Main product yields for real textile waste at StC of 0.8.

	Unit	707 °C	755 °C	802 °C	853 °C
$CO + H_2$	wt.% $_{(daf)}$	31.6	30.4	36.2	38.8
CH_4	wt.% $_{(daf)}$	5.62	5.69	6.85	6.64
$C_2H_4 + C_3H_6$	wt.% $_{(daf)}$	7.51	6.37	6.57	4.98
Benzene + toluene (B + T)	wt.% $_{(daf)}$	7.89	10.4	9.85	7.48

Syngas is used in the production of various fuels and chemicals, such as ammonia, methanol and dimethyl ether (DME), H_2, hydrocarbon fuels (via Fischer-Tropsch synthesis) as well as olefins (from methanol) for the production of new polymers [20,69–73]. For the production of methanol from syngas the molar ratio $(H_2 - CO_2)/(CO + CO_2)$ should be optimized to give a value of two or slightly above two. The ratio is referred to the M−modulus or R ratio and is used as a metric to gauge the suitability of syngas for methanol production [19,74]. For the real textile waste stream, the M−modulus was between 0.2 and 0.3 for temperatures between 707 and 853 °C, however with downstream processing, such as WGS and CO_2 removal, the ratio can be increased to the desired value for methanol production.

Benzene, is a high-value chemical used in various industries as a fuel and a building block for new plastics, dyes, lubricants and synthetic fibres (such as polyester) [75]. The production of new fibres through thermochemically recycled textile assists with the transition towards a circular economy (fibre to fibre). In addition, to syngas and B + T, olefins (at lower operating temperatures; < 750 °C) and CH_4 were retrieved to a lesser extent. These components are of value to the chemical industry for the production of new polymers (from C_2H_4 and C_3H_6). CH_4 is a substitute for natural gas or can be used for the production of syngas via steam reforming [12,76]. Thermochemical recycling of textile waste offers the potential to retrieve products via different routes. All products (or a fraction of the various products e.g. B + T and syngas) can be retrieved via a downstream cascade approach, or one product can be targeted through optimization of process conditions and downstream conversion of the other products. This chemical recycling technique can thus be integrated with different processes, depending on the target applications of the product, making it a versatile process.

A challenge with the thermochemical textile recycling is that CO_2 is also produced, mainly due to decomposition of PET. Depending on the target application, the CO_2 should be fully or partially removed from the product gas. For the production of methanol, some CO_2 in the product is favourable for the equilibrium (2 – 5 vol%) [73,77]. Different techniques exist for the removal of CO_2 from the product gas, which can either be used in other processes or stored. For example, the removed CO_2 can be used as reactant with green hydrogen for the production of other valuable fuels and chemicals such as methanol, methane and olefins [78]. Another challenge is the presence of contaminants, namely nitrogen from polymers (such as PA6, PUR, polyacrylics etc.), halogens (e.g. bromide from fire retardants and chloride), sulphur and other inorganics originating from dyes and other additives used during the textile manufacturing process. During thermochemical conversion, these contaminants are distributed over the various product streams (gas, solids and liquids). The nitrogen content predominantly ends in the product gas as NH_3 and HCN in the presence of steam (see Section 3.2.3), while the remaining fraction goes to the condensable or solid phase. The first results showed that the concentration of H_2S in the product gas was low and it is assumed that the majority of the sulphur is retained in the solid phase. Research is required to map the contaminant distribution and develop strategies for downstream processing to reduce emissions and for the integration with existing chemical processes. Having an overview of the contaminants will also aid textile producers in rethinking the design for better recyclability, such as selecting additives during the fabrication to reduce contaminants released during recycling. Lastly, looking at the volumes and availability of textile waste, it would be beneficial to consider blending textile waste with post-consumer plastics waste streams for the production of high-value chemicals via thermal cracking. Thermal cracking of plastic waste is a robust technology able to handle various heterogenous waste streams with minimal pre-treatment [79]. Alternatively, textile waste streams containing high

concentrations of cotton, such as workwear, can be blended with biogenic waste for the production of new bio-based chemicals and materials via gasification.

5. Conclusions

The thermochemical behaviour of model mixtures and real textile waste was experimentally investigated under various conditions (temperatures and steam flows). The aim was to compare the product distributions and evaluate the viability of applying thermochemical methods as treating pathways for textile waste valorisation, to retrieve products for the productions of new textiles or for fuels and chemicals. The model mixtures which were rich in PET (80 – 100 %) mainly yielded CO_2 and aromatics (mainly benzene), due to the thermal decomposition of PET. The addition of PA6 and PUR increased the hydrocarbons yield and decreased the CO_2, and benzene yields due to the reduced PET content in the feedstock. For the model mixtures at 700 °C, the participation of steam was minimal, and product distribution mainly resulted from the thermal decomposition of the polymers. For the real textile waste (±58 wt% cotton) the product distribution shifted towards more gaseous products, predominantly syngas. The chemical structure of the polymers and cotton play a crucial role in the product distribution, leading to the cotton-rich textile waste yielding more syngas and hydrocarbons (CH_4 and C_2H_4), and the PET-rich model mixtures yielding more aromatics (benzene and toluene) and CO_2. Higher reaction temperatures, for real textile waste, initially enhanced the B + T and C_2H_4 yields, but as the temperature continued to increase more syngas was produced, due to increased steam participation from steam reforming reactions. At 853 °C, the presence of steam mainly affected H_2 and CO_2 yields, both increasing with 50 %. For the nitrogen containing species, the majority of the nitrogen goes towards the formation of NH_3 and HCN in the product gas in the presence of steam.

Overall, the main products retrieved from real textile waste are syngas and for lower temperatures (up to 802 °C) B + T and olefins. The diverse product slate of thermochemical textile processing presents different opportunities for integration with various chemical industries. A first step has been taken to measure the concentration of contaminants such as NH_3, HCN and H_2S in the product gas. A next step in the development of the thermochemical recycling would be to measure and quantify the distribution of the contaminants in the condensable and solid phase to have a complete nitrogen and sulphur balance. The development should also include the measurement of other contaminants such as halogens (chloride and bromide) in the different phases. The analysis scope should be expanded to include the analysis of oxygen and nitrogen components in the condensables to better quantify the degradation products of the polymers. This in turn can be leveraged for the development of methods and downstream processes to remove contaminants and purify the product stream for other applications. Additionally, the results could steer the development of new textiles, where the right additives can have a positive effect on the recyclability of the material. The results of this study demonstrate the feasibility of using thermochemical conversion for the treatment of mixed textile waste to retrieve high-value and versatile products, reducing textile waste and transitioning towards a circular economy.

CRediT authorship contribution statement

Surika van Wyk: Writing – original draft, Validation, Methodology, Investigation, Formal analysis, Data curation, Conceptualization. **Carlos F. Mourao Vilela:** Writing – review & editing, Project administration, Methodology, Funding acquisition, Conceptualization. **Berend J. Vreugdenhil:** Writing – review & editing, Resources.

Declaration of competing interest

The authors declare that they have no known competing financial interests or personal relationships that could have appeared to influence the work reported in this paper.

Acknowledgements

The authors would like to thank Vincent Vink for preparing the textile feedstock, Marco Geusebrock, and Arnold Toonen for the sampling and sample analysis during the experiments and Mark Visser and Carel Meijwes for preparation, maintenance and operation of the installation for the experiments. The authors would also like to thank the Boer Group (Textile recycling with purpose & innovation by tradition) for providing the real mixed textile waste and the Dutch Ministry of Economic Affairs and Climate Policy for funding the research.

Appendix A. Supplementary data

Supplementary data to this article can be found online at https://doi.org/10.1016/j.fuel.2025.137564.

Data availability

Data will be made available on request.

References

[1] Bianchi S, Bartoli F, Bruni C, Fernandez-Avila C, Rodriguez-Turienzo L, Mellado-Carretero J, et al. Opportunities and limitations in recycling fossil polymers from textiles. Macromol 2023;3:120–48. https://doi.org/10.3390/macromol3020009.
[2] Eder-Hansen, Jonas, Chalmer, Caroline, Tarneberg, Sofia, Tochtermann, Thomas, Seara, Javier, Boger, Sebastian, Theelen, Gabriele, Schwarz, Sebastian, Kristensen, Lise, Jager, Kristina, Pulse of the fashion industry, Global fashion agenda & The Boston consulting group, 2017. https://www.greylockglass.com/wp-content/uploads/2021/08/Pulse-of-the-Fashion-Industry_2017.pdf (accessed December 12, 2024).
[3] Ellen MacArthur Foundation, A new textiles economy: Redesigning fashion's future, Ellen MacArthur Foundation, 2017. https://www.ellenmacarthurfoundation.org/publications (accessed December 12, 2024).
[4] Clark JH. Textile waste – an opportunity as well as a threat, Green. Carbon 2023;1:146–9. https://doi.org/10.1016/j.greenca.2023.10.002.
[5] Tripathi M, Sharma M, Bala S, Thakur VK, Singh A, Dashora K, et al. Recent technologies for transforming textile waste into value-added products: a review. Curr Res Biotechnol 2024;7:100225. https://doi.org/10.1016/j.crbiot.2024.100225.
[6] Athanasopoulos P, Zabaniotou A. Post-consumer textile thermochemical recycling to fuels and biocarbon: a critical review. Sci Total Environ 2022;834:155387. https://doi.org/10.1016/j.scitotenv.2022.155387.
[7] Baloyi RB, Gbadeyan OJ, Sithole B, Chunilall V. Recent advances in recycling technologies for waste textile fabrics: a review. Text Res J 2024;94:508–29. https://doi.org/10.1177/00405175231210239.
[8] Juanga-Labayen JP, Labayen IV, Yuan Q. A review on textile recycling practices and challenges. Textiles 2022;2:174–88. https://doi.org/10.3390/textiles2010010.
[9] Matayeva A, Dos Passos JS, Straka P, Skibsted SKG, Biller P. Chemical recycling of post-consumer textile waste via continuous hydrothermal liquefaction and hydrotreatment for simultaneous monomer and hydrocarbons production. Chem Eng J 2025;508:161108. https://doi.org/10.1016/j.cej.2025.161108.
[10] Zhuang X, Zhu N, Li F, Lin H, Liang C, Dang Z, et al. Hydrogen-rich syngas production from waste textile gasification coupling with catalytic reforming under steam atmosphere. Processes 2024;12:1790. https://doi.org/10.3390/pr12091790.
[11] Lange JP, Kersten SRA, Meester SD, Ragaert K. Plastic recycling stripped naked – from circular product to circular industry with recycling cascade, (2024).
[12] Dogu O, Pelucchi M, Van De Vijver R, Van Steenberge PHM, D'hooge DR, Cuoci A, Mehl M, Frassoldati A, Faravelli T, Van Geem KM. The chemistry of chemical recycling of solid plastic waste via pyrolysis and gasification: State-of-the-art, challenges, and future directions. Prog. Energy Combust. Sci. 2021;84:100901. https://doi.org/10.1016/j.pecs.2020.100901.
[13] Kaminsky W. Chemical recycling of plastics by fluidized bed pyrolysis. Fuel Commun 2021;8:100023. https://doi.org/10.1016/j.jfueco.2021.100023.
[14] Yang Y, Shahbeik H, Shafizadeh A, Rafiee S, Hafezi A, Du X, et al. Predicting municipal solid waste gasification using machine learning: a step toward sustainable regional planning. Energy 2023;278:127881. https://doi.org/10.1016/j.energy.2023.127881.
[15] Cho M-H, Jung S-H, Kim J-S. Pyrolysis of mixed plastic wastes for the recovery of benzene, toluene, and xylene (BTX) aromatics in a fluidized bed and chlorine removal by applying various additives. Energy Fuels 2010;24:1389–95. https://doi.org/10.1021/ef901127v.

[16] Alfè M, Gargiulo V, Porto M, Migliaccio R, Le Pera A, Sellaro M, et al. Pyrolysis and gasification of a real refuse-derived fuel (RDF): the potential use of the products under a circular economy vision. Molecules 2022;27:8114. https://doi.org/10.3390/molecules27238114.
[17] Lopez G, Artetxe M, Amutio M, Bilbao J, Olazar M. Thermochemical routes for the valorization of waste polyolefinic plastics to produce fuels and chemicals. A review. Renew Sustain Energy Rev 2017;73:346–68. https://doi.org/10.1016/j.rser.2017.01.142.
[18] Lopez G, Artetxe M, Amutio M, Alvarez J, Bilbao J, Olazar M. Recent advances in the gasification of waste plastics. A critical overview. Renew Sustain Energy Rev 2018;82:576–96. https://doi.org/10.1016/j.rser.2017.09.032.
[19] Mandviwala C, Forero Franco R, Berdugo Vilches T, Gogolev I, González-Arias J, Cañete Vela I, et al. Steam cracking in a semi-industrial dual fluidized bed reactor: tackling the challenges in thermochemical recycling of plastic waste. Chem Eng J 2024;500:156892. https://doi.org/10.1016/j.cej.2024.156892.
[20] Cañete Vela I, Maric J, Seeman M, Valorisation of textile waste via steam gasification in a fluidized bed reactor, in: HERAKLION 2019, 2019.
[21] Yasin S, Massimo C, Rovero G, Behary N, Perwuelz A, Giraud S, Migliavacca G, Chen G, Guan J. An alternative for the end-of-life phase of flame retardant textile products: degradation of flame retardant and preliminary settings of energy valorization by gasification. BioResources 2017;12:5196–211. https://doi.org/10.15376/biores.12.3.5196-5211.
[22] Yasin S, Curti M, Rovero G, Hussain M, Sun D. Spouted-bed gasification of flame retardant textiles as a potential non-conventional biomass. Appl Sci 2020;10:946. https://doi.org/10.3390/app10030946.
[23] Wen C, Wu Y, Chen X, Jiang G, Liu D. The pyrolysis and gasification performances of waste textile under carbon dioxide atmosphere. J Therm Anal Calorim 2017;128:581–91. https://doi.org/10.1007/s10973-016-5887-7.
[24] Lee HS, Jung S, Lin K-Y-A, Kwon EE, Lee J. Upcycling textile waste using pyrolysis process. Sci Total Environ 2023;859:160393. https://doi.org/10.1016/j.scitotenv.2022.160393.
[25] Sina Ogundaini R, Monsurat Osobamiro T. Textile waste pyrolysis: an innovative method for petrochemicals generation for sustainable economic, technological and environmental advancement. Environ Sci Pollut Res 2024;31:65627–37. https://doi.org/10.1007/s11356-024-35617-4.
[26] Arjona L, Barrós I, Montero Á, Solís RR, Pérez A, Martín-Lara MÁ, et al. Pyrolysis of textile waste: a sustainable approach to waste management and resource recovery. J Environ Chem Eng 2024;12:114730. https://doi.org/10.1016/j.jece.2024.114730.
[27] Niu M, Huang Y, Jin B, Wang X. Oxygen Gasification of Municipal Solid Waste in a Fixed-bed Gasifier. Chin J Chem Eng 2014;22:1021–6. https://doi.org/10.1016/j.cjche.2014.06.026.
[28] Gracia-Monforte C, Zapata G, Afailal Z, Gea G, Arauzo J. Textile waste valorization via gasification: a comparative experimental study of different gasifying agents. Biomass Bioenergy 2025;199:107905. https://doi.org/10.1016/j.biombioe.2025.107905.
[29] Forero-Franco R, Cañete-Vela I, Berdugo-Vilches T, Mandviwala C, Perez ND, Gogolev I, et al. Towards sustainable textile waste management: Exploring valuable chemicals production through steam cracking in a dual fluidized bed. Fuel 2025;397:135731. https://doi.org/10.1016/j.fuel.2025.135731.
[30] Circular economy, Biomimicry institue, Design for transformation, Cricular economy, Rotterdam, 2024. https://www.circle-economy.com/resources/design-for-transformation (accessed December 12, 2024).
[31] Moreno-Marrodán C, Brandi F, Barbaro P, Liguori F. Advances in catalytic chemical recycling of synthetic textiles. Green Chem 2024;26:11832–59. https://doi.org/10.1039/D4GC04768K.
[32] Pavan M, Samant L, Mahajan S, Kaur M, Role of Chemicals in Textile Processing and Its Alternatives, in: Clim. Action Eco-Friendly Text., Springer International Publishing, 2024: pp. 55–75. https://link.springer.com/chapter/10.1007/978-981-99-9856-2_5#citeas.
[33] Van de Kamp WL, De Wild PJ, Knoef HAM, Neeft JPA, Kiel JHA, Tar measurement in biomass gasification, standardisation and supporting R&D, TNO (past ECN), 2006. https://publications.tno.nl/publication/34628627/3oZ90f/c06046.pdf (accessed March 6, 2024).
[34] Buentello-Montoya DA, Duarte-Ruiz CA, Maldonado-Escalante JF. Co-gasification of waste PET, PP and biomass for energy recovery: a thermodynamic model to assess the produced syngas quality. Energy 2023;266:126510. https://doi.org/10.1016/j.energy.2022.126510.
[35] Aranda Almansa G, Mourao Vilela C, Vreugdenhil BJ. Gas analysis in gasification of biomass and waste Guideline report Document 1. IEA Bioenergy 2018.
[36] van Paasen SVB, Kiel JHA, Tar formation in fluidised-bed gasification - Impact of gasifier operating conditions, in: 2nd World Conf. Technol. Exhib. Biomass Energy Ind. Clim. Prot., Rome, Italy, 2004.
[37] Oenema J, Liu H, Coensel ND, Eschenbacher A, Van De Vijver R, Weng J, et al. Review on the pyrolysis products and thermal decomposition mechanisms of polyurethanes. J Anal Appl Pyrol 2022;168:105723. https://doi.org/10.1016/j.jaap.2022.105723.
[38] Font R, Fullana A, Caballero JA, Candela J, García A. Pyrolysis study of polyurethane. J Anal Appl Pyrolysis 58–59 2001:63–77. https://doi.org/10.1016/S0165-2370(00)00138-8.
[39] Robinson T, Bronson B, Gogolek P, Mehrani P. Comparison of the air-blown bubbling fluidized bed gasification of wood and wood–PET pellets. Fuel 2016;178:263–71. https://doi.org/10.1016/j.fuel.2016.03.038.
[40] Li S, Cañete Vela I, Järvinen M, Seemann M. Polyethylene terephthalate (PET) recycling via steam gasification – the effect of operating conditions on gas and tar composition. Waste Manag 2021;130:117–26. https://doi.org/10.1016/j.wasman.2021.05.023.
[41] Brems A, Baeyens J, Vandecasteele C, Dewil R. Polymeric cracking of waste polyethylene terephthalate to chemicals and energy. J Air Waste Manag Assoc 2011;61:721–31. https://doi.org/10.3155/1047-3289.61.7.721.
[42] Gong L, Pan Y, Cui L, Zhang X. Atomic insights into the thermal degradation of polyethylene terephthalate combining STA-FTIR and DFT methods. Fuel 2024;364:131067. https://doi.org/10.1016/j.fuel.2024.131067.
[43] Wilk V, Hofbauer H. Conversion of mixed plastic wastes in a dual fluidized bed steam gasifier. Fuel 2013;107:787–99. https://doi.org/10.1016/j.fuel.2013.01.068.
[44] Kumagai S, Yabuki R, Kameda T, Saito Y, Yoshioka T. Simultaneous recovery of H2-rich syngas and removal of HCN during pyrolytic recycling of polyurethane by Ni/Mg/Al catalysts. Chem Eng J 2019;361:408–15. https://doi.org/10.1016/j.cej.2018.12.099.
[45] Kumagai S, Hosaka T, Kameda T, Yoshioka T. Removal of toxic HCN and recovery of H2-rich syngas via catalytic reforming of product gas from gasification of polyimide over Ni/Mg/Al catalysts. J Anal Appl Pyrol 2017;123:330–9. https://doi.org/10.1016/j.jaap.2016.11.012.
[46] Chen G, Liu T, Luan P, Li N, Sun Y, Tao J, et al. Distribution, migration, and removal of N-containing products during polyurethane pyrolysis: a review. J Hazard Mater 2023;453:131406. https://doi.org/10.1016/j.jhazmat.2023.131406.
[47] Ren P, Li T, Feng L, Gu X, Jiang M, Duan J, et al. Thermal degradation of polyamide 6: mechanisms, mitigation strategies, and challenges. Chem Eng Sci 2025;316:121985. https://doi.org/10.1016/j.ces.2025.121985.
[48] Kaminsky W, Feedstock recycling of nitrogen containing polymers by fluidized bed pyrolysis, (n.d.).
[49] Akah A, Williams J, Ghrami M. An overview of light olefins production via steam enhanced catalytic cracking. Catal Surv Asia 2019;23:265–76. https://doi.org/10.1007/s10563-019-09280-6.
[50] Herrera M, Matuschek G, Kettrup A. Thermal degradation studies of some aliphatic polyamides using hyphenated techniques (TG-MS, TG-FTIR). J Therm Anal Calorim 2000;59:385–94. https://doi.org/10.1023/A:1010177105297.
[51] Forero-Franco R, Cañete-Vela I, Berdugo-Vilches T, González-Arias J, Maric J, Thunman H, et al. Correlations between product distribution and feedstock composition in thermal cracking processes for mixed plastic waste. Fuel 2023;341:127660. https://doi.org/10.1016/j.fuel.2023.127660.
[52] Leichtnam J-N, Schwartz D, Gadiou R. The behaviour of fuel-nitrogen during fast pyrolysis of polyamide at high temperature. J Anal Appl Pyrol 2000;55:255–68. https://doi.org/10.1016/S0165-2370(00)00075-9.
[53] Westerhout RWJ, Kuipers JAM, Van Swaaij WPM. Experimental determination of the yield of pyrolysis products of polyethene and polypropene. Influence of reaction conditions. Ind Eng Chem Res 1998;37:841–7. https://doi.org/10.1021/ie970384a.
[54] Abbas-Abadi MS. The effect of process and structural parameters on the stability, thermo-mechanical and thermal degradation of polymers with hydrocarbon skeleton containing PE, PP, PS, PVC, NR, PBR and SBR. J Therm Anal Calorim 2021;143:2867–82. https://doi.org/10.1007/s10973-020-09344-0.
[55] Lahtinen J, Hashmi F, Taavitsainen V-M. Temperature-dependent pyrolysis of polyamide–polyethylene multilayer films: yields, monomer recovery, and product boiling range. Energy Fuels 2025;39:16956–67. https://doi.org/10.1021/acs.energyfuels.5c02329.
[56] Shen D, Xiao R, Gu S, Luo K. The pyrolytic behavior of cellulose in lignocellulosic biomass: a review. RSC Adv 2011;1:1641. https://doi.org/10.1039/c1ra00534k.
[57] Wei Z, Li Y, Zhang C, Yang L, Chu L. Revealing the mechanism on steam co-gasification of cellulose and polyethylene: a combined ReaxFF and DFT study. Fuel 2023;334:126784. https://doi.org/10.1016/j.fuel.2022.126784.
[58] Fukutome A, Kawamoto H, Saka S. Processes forming gas, tar, and coke in cellulose gasification from gas-phase reactions of levoglucosan as intermediate. ChemSusChem 2015;8:2240–9. https://doi.org/10.1002/cssc.201500275.
[59] Li C, Sun Y, Li Q, Zhang L, Zhang S, Wang H, et al. Effects of volatiles on properties of char during sequential pyrolysis of PET and cellulose. Renew Energy 2022;189:139–51. https://doi.org/10.1016/j.renene.2022.02.091.
[60] Ma SM, Zou C, Chen T-Y, Paulson JA, Lin L-C, Bakshi BR. Understanding rapid PET degradation via reactive molecular dynamics simulation and kinetic modeling. Chem A Eur J 2023;127:7323–34. https://doi.org/10.1021/acs.jpca.3c03717.
[61] Wu C, Wang Z, Huang J, Williams PT. Pyrolysis/gasification of cellulose, hemicellulose and lignin for hydrogen production in the presence of various nickel-based catalysts. Fuel 2013;106:697–706. https://doi.org/10.1016/j.fuel.2012.10.064.
[62] Zhou H, Wu C, Onwudili JA, Meng A, Zhang Y, Williams PT. Polycyclic aromatic hydrocarbons (PAH) formation from the pyrolysis of different municipal solid waste fractions. Waste Manag 2015;36:136–46. https://doi.org/10.1016/j.wasman.2014.09.014.
[63] Cortazar M, Santamaria L, Lopez G, Alvarez J, Zhang L, Wang R, et al. A comprehensive review of primary strategies for tar removal in biomass gasification. Energy Convers Manag 2023;276:116496. https://doi.org/10.1016/j.enconman.2022.116496.
[64] Wang W, Li Q, Wang Q, Zhang J, Liu J. Tar steam reforming during biomass gasification: kinetic model and reaction pathway, Clean Technol. Environ. Policy 2022;24:39–50. https://doi.org/10.1007/s10098-021-02062-7.
[65] Golombok M, Van Der Bijl J, Kornegoor M. Severity parameters for steam cracking. Ind Eng Chem Res 2001;40:470–2. https://doi.org/10.1021/ie990436r.
[66] Mollick M, Santamaria L, Cortazar M, Mollick PK, Comendador P, Amutio M, et al. Evaluation of temperature role in the HDPE steam cracking product distribution

with a focus on light olefins production. J Anal Appl Pyrol 2025;186:106922. https://doi.org/10.1016/j.jaap.2024.106922.
[67] Hongrapipat J, Pang S, Saw WL. Removal of NH3 and H2S from producer gas in a dual fluidised bed steam gasifier by optimisation of operation conditions and application of bed materials. Biomass Convers Biorefinery 2016;6:105–13. https://doi.org/10.1007/s13399-015-0167-5.
[68] Morrin S, Lettieri P, Chapman C, Mazzei L. Two stage fluid bed-plasma gasification process for solid waste valorisation: Technical review and preliminary thermodynamic modelling of sulphur emissions. Waste Manag 2012;32:676–84. https://doi.org/10.1016/j.wasman.2011.08.020.
[69] Flórez-Orrego D, De Oliveira Junior S. On the efficiency, exergy costs and CO 2 emission cost allocation for an integrated syngas and ammonia production plant. Energy 117 2016:341–60. https://doi.org/10.1016/j.energy.2016.05.096.
[70] Mahmoudi E, Sayyah A, Farhoudi S, Bahranifard Z, Behmenyar G, Turan AZ, et al. Advances in catalysts for direct syngas conversion to light olefins: a review of mechanistic and performance insights. J CO2 Util 2024;86:102893. https://doi.org/10.1016/j.jcou.2024.102893.
[71] Svanberg M, Ellis J, Lundgren J, Landälv I. Renewable methanol as a fuel for the shipping industry. Renew Sustain Energy Rev 2018;94:1217–28. https://doi.org/10.1016/j.rser.2018.06.058.
[72] Seddon D, Methanol and dimethyl ether (DME) production from synthesis gas, in: Adv. Clean Hydrocarb. Fuel Process, Elsevier, 2011: pp. 363–386. doi: 10.1533/9780857093783.4.363.
[73] Luk HT, Mondelli C, Ferré DC, Stewart JA, Pérez-Ramírez J. Status and prospects in higher alcohols synthesis from syngas. Chem Soc Rev 2017;46:1358–426. https://doi.org/10.1039/C6CS00324A.
[74] Brachi P, Chirone R, Miccio F, Miccio M, Picarelli A, Ruoppolo G. Fluidized bed co-gasification of biomass and polymeric wastes for a flexible end-use of the syngas: Focus on bio-methanol. Fuel 2014;128:88–98. https://doi.org/10.1016/j.fuel.2014.02.070.
[75] Wang J, Jiang J, Sun Y, Zhong Z, Wang X, Xia H, et al. Recycling benzene and ethylbenzene from in-situ catalytic fast pyrolysis of plastic wastes. Energy Convers Manag 2019;200:112088. https://doi.org/10.1016/j.enconman.2019.112088.
[76] Gunawardane K, Evolution of hydrogen energy and its potential opportunities around the globe, in: Hydrog. Energy Convers. Manag., Elsevier, 2024: pp. 3–33. 10.1016/B978-0-443-15329-7.00007-7.
[77] Ott J, Gronemann V, Pontzen F, Fiedler E, Grossmann G, Kersebohm F, Weiss F, Witte C, Methanol, in: Wiley-VCH (Ed.), Ullmanns Encycl. Ind. Chem., 1st ed., Wiley, 2012. doi: 10.1002/14356007.a16_465.pub3.
[78] Minyukova TP, Dokuchits EV. Hydrogen for CO2 processing in heterogeneous catalytic reactions. Int J Hydrog Energy 2023;48:22462–83. https://doi.org/10.1016/j.ijhydene.2023.03.264.
[79] Thunman H, Berdugo Vilches T, Seemann M, Maric J, Vela IC, Pissot S, et al. Circular use of plastics-transformation of existing petrochemical clusters into thermochemical recycling plants with 100% plastics recovery. Sustain Mater Technol 2019;22:e00124. https://doi.org/10.1016/j.susmat.2019.e00124.